



ELSEVIER

Contents lists available at ScienceDirect

Journal of Magnetism and Magnetic Materials

journal homepage: www.elsevier.com/locate/jmmm

Influence of cobalt doping on the hyperthermic efficiency of magnetite nanoparticles

Elvira Fantechi^a, Claudia Innocenti^a, Martin Albino^a, Elisabetta Lottini^a, Claudio Sangregorio^{b,*}^a INSTM and Department of Chemistry "U. Schiff", Università di Firenze, via della Lastruccia 3, Sesto Fiorentino, I-50019 Firenze, Italy^b C.N.R. – I.C.C.O.M., via Madonna del Piano 10, I-50019 Sesto Fiorentino, Italy

ARTICLE INFO

Article history:

Received 9 July 2014

Received in revised form

14 October 2014

Accepted 18 October 2014

Available online 22 October 2014

Keywords:

Magnetic fluid hyperthermia

Specific Absorption Rate

Cobalt ferrite

Magnetic nanoparticle

Magnetic anisotropy

ABSTRACT

Magnetite nanoparticles (NPs) are extensively investigated for biomedical applications, particularly as contrast agents for Magnetic Resonance Imaging and as heat mediators in Magnetic Fluid Hyperthermia. For the latter, one of the goal of the research is to obtain materials with improved hyperthermic properties. A valuable strategy is the increase of the magnetic anisotropy of commonly employed magnetite through the total or partial substitution of Fe^{2+} ions with Co^{2+} ions. Here we present a study on a family of 8 nm Co-doped magnetite NPs ($\text{Co}_x\text{Fe}_{3-x}\text{O}_4$), with composition ranging from pure magnetite ($x=0$) to stoichiometric cobalt ferrite ($x=1$), aimed to investigate the evolution of the hyperthermic properties with the increase of Co content. We found that the addition of a small amount of Co is enough to sharply increase the Specific Absorption Rate (SAR). The SAR further increases with x but it reaches a maximum for an intermediate value ($x=0.6$). Such anomalous behavior is ascribed to the intrinsic magnetic properties of the material, and, in particular, to the magnetic anisotropy, which displays the same peculiar trend. The Co-doping thus may represent an effective strategy to improve the poor hyperthermic efficiency of very small magnetite NPs (< 10 nm).

© 2014 Elsevier B.V. All rights reserved.

1. Introduction

One of the most intriguing properties of magnetic nanoparticles (NPs) is the capability to generate heat under an alternating magnetic field thanks to the energy losses occurring during the magnetization reversal [1–3]. This property is the base of a promising application in biomedicine, known as Magnetic Fluid Hyperthermia (MFH), which can be employed as anticancer therapy by thermal ablation or, since cancerous cells are more sensitive to heat than healthy ones, by apoptosis or as coadjuvant for chemo- and radio-therapies [4,5]. In comparison with other hyperthermic treatments, MFH offers a better selectivity as the heat is locally generated in the tissue where the NPs accumulate. Moreover, in principle MFH could be conjugated with Magnetic Resonance Imaging (MRI) providing the opportunity to build up a theranostic nanosystem able to diagnose, treat and monitor the cancer evolution during the therapy. The multifold properties of magnetic NPs can be further exploited by the widespread functionalization reactions at the NPs surface which confer tailored

properties depending on the target application of the nanosystem [3,6].

Among the parameters which can be tuned to optimize the hyperthermic efficiency, the mean size of NPs is one of the most effective [7,8]. The optimal size, however, depends on the composition of the selected material. As instance, for iron oxide ferrites, i.e. magnetite (Fe_3O_4) and maghemite ($\gamma\text{-Fe}_2\text{O}_3$), which have been the first and most investigated materials for biomedical applications because of their biocompatibility, the optimal size is around 12–24 nm, depending on the oxidation degree and on the applied frequency [7–11]. A further reduction of the particle size is one of the challenges in the material research for biomedical applications since smaller systems are expected to better avoid the immunitary system and have a longer circulation time in blood vessels, thus increasing the probability to target the tumor tissue. In addition, for magnetic carriers, small NPs are more stable against aggregation, avoiding precipitation and consequently the risk of blood vessel occlusion. In order to reduce the NP size while increasing or at least keeping constant the hyperthermic efficiency obtained with the traditional iron ferrites, the research has then to focus on alternative materials. A straight strategy to achieve this goal is to increase the magnetic anisotropy of iron oxide-based materials by replacing, for example, the divalent iron with a more anisotropic cation, like cobalt. It has been already demonstrated,

* Corresponding author. Fax: +39 0554573327.

E-mail address: csangregorio@iccom.cnr.it (C. Sangregorio).

indeed, that small sized NPs ($d < 12$ nm) of cobalt ferrite (CoFe_2O_4), which bulk anisotropy constant is *ca.* 20–30 times greater than magnetite, have a larger hyperthermic and MRI contrast efficiency than magnetite NPs of the same size [7,12]. Despite the promising properties of this material, its use in bio-medical application is debated due to the presence of cobalt. While for uncoated cobalt ferrite NPs a non-negligible toxicity is reported in the literature [13,14], the coating with silica or polymers strongly improves their biocompatibility [13,15,16]. However, a low residual toxicity is often still present, depending on the cellular line investigated and on the concentration of the NPs used [17,18]. Moreover, it must be noted that almost all cytotoxicity tests reported in the literature are performed at much lower NPs concentrations than that required by hyperthermia assays. The release of free cobalt ions from the NPs (leaching) is reported in several works, the amount of cobalt released depending on the concentration, on the coating and on the experimental conditions of the tests [17,19,20]. Moreover, another possible source of toxicity is the Co release occurring during the biodegradation of those NPs that have not completely excreted from kidneys, liver or other excretion pathways. In this manifold scenario, the presence of cobalt could in some cases represent a potential source of toxicity, in particular if large amounts of NPs or high concentration are used. A controlled reduction of cobalt content can thus represent a suitable compromise between the needs of limiting the potential toxicity and the advantage of the aforementioned properties of a strong anisotropic material. Indeed, in a recent study of Co-doped NPs grown in the internal cavity of functionalized human ferritin, some of us demonstrated that a small amount of doping (5% w/w) was enough to strongly enhance the hyperthermic efficacy on melanoma cells with respect to the undoped samples, without compromising the cytotoxicity of the material [21]. Moreover, some of us reported that the magnetic anisotropy of 5 nm $\text{Co}_x\text{Fe}_{(8/3-2/3x)}\text{O}_4$ NPs does not increase monotonously with Co reaching a maximum for intermediate composition ($x=0.6$) [22]. These results suggest the possibility to reduce significantly the Co content while achieving performances that match and even out-class those of stoichiometric cobalt ferrite. Although nanocrystalline cobalt ferrite has already been investigated for application in MHF [7,12,23,24], to our knowledge no attention has been paid to the dependence of the hyperthermic efficiency on the cobalt content.

Here we report the synthesis and characterization of a family of 8 nm non-stoichiometric cobalt ferrite, $\text{Co}_x\text{Fe}_{3-x}\text{O}_4$ with $0 \leq x \leq 1.0$ and the investigation of their ability to generate heat under an alternating magnetic field. Samples were synthesized by thermal decomposition of metal acetylacetonates in high-boiling solvents in the presence of surfactants. This method allows for obtaining high crystalline, size-controlled MNPs with tuned composition from magnetite to stoichiometric cobalt ferrite. The hyperthermic efficiency of the obtained samples was found to have a non-monotonous trend with Co-content, reaching maximum values for the intermediate composition $x=0.6$. A complete structural and magnetic characterization was performed in order to correlate this peculiar behavior with the properties of the material.

2. Materials and methods

2.1. Synthesis

All the samples were prepared under inert atmosphere using commercially available reagents. Hexane (99%), phenyl ether (Ph_2O , 99%), benzyl ether (Bn_2O , 99%), 1,2-hexadecanediol (HDD) (97%), oleic acid (OA) (90%), oleylamine (OAM) (70%), lauric acid

(LA) and cobalt(II) acetylacetonate (97%) were purchased from Aldrich Chemical Co. and Iron(III) acetylacetonate (99%) from Strem Chemicals, Inc. Absolute ethanol was from Fluka. All chemicals were used as received.

In a typical synthesis, $\text{Fe}(\text{acac})_3$ and $\text{Co}(\text{acac})_2$ (in various proportions, 1 mmol total), OA (0.64 ml, 2 mmol), OAM (0.64 ml, 2 mmol) and HDD (0.67 g, 2.3 mmol) were mixed and magnetically stirred under a flow of nitrogen in Ph_2O (30 ml). The mixture was kept at 200 °C for 2 h under a blanket of nitrogen and vigorously stirred, then heated to reflux for 1 h. The black-brown mixture was cooled down to room temperature and EtOH was added to the mixture, under ambient conditions, causing the precipitation of a black powder which was separated *via* centrifugation (5000 rpm, 10 min). The black product was dispersed by sonication in EtOH several times, then centrifuged (5000 rpm, 10 min) and dried. The product could be readily dispersed into hexane.

Samples with different metal compositions were obtained by modifying the initial metal ratio in the reaction synthesis. However, since the effective metal Co:Fe ratio was found systematically lower than the nominal one (see discussion below, Section 3.1), the reaction conditions were modified to increase the incorporation of Co in the final products by changing the kind and amount of surfactants and/or the solvent used (benzyl ether or phenyl ether). The experimental conditions used for the synthesis of the different samples are reported in Table 1.

In the following, the synthesized $\text{Co}_x\text{Fe}_{3-x}\text{O}_4$ samples will be labeled as CoFe $_{zz}$, where z is the cobalt content (i.e. $zz=06$ for $x=0.6$).

2.2. Structural characterization

Size and morphology of the NPs were determined by Transmission Electron Microscopy (TEM), using a CM12 PHILIPS microscope operating at 100 kV. Samples were prepared by drop drying a diluted suspension of NPs in hexane onto 200 mesh carbon-coated copper grids. The recorded images were analyzed with the Image Pro-Plus[®] software. The mean diameter and the size distribution of each sample were obtained from a statistical analysis over 500–900 particles.

Powder X-Ray Diffraction (XRD) measurements were carried out using a Bruker D8 Advance diffractometer equipped with a $\text{CuK}\alpha$ radiation and operating in θ - 2θ Bragg Brentano geometry at 40 kV and 40 mA. Lattice parameters, a , and mean crystallite diameters, d_{XRD} , were evaluated using the TOPAS[®] software (Bruker) by the method of Fundamental Parameter Approach considering a cubic spatial group $Fd3m$.

ICP-AES measurements were performed in triplicate by a Varian 720-ES Inductively Coupled Plasma Atomic Emission Spectrometer (ICP-AES). For the analysis, about 1 mg of sample was digested by concentrated aqua regia (HCl suprapure and HNO_3 sub-boiled in 3:1 ratio) in the presence of H_2O_2 , diluted with ultrapure water ($\geq 18 \Omega$) and then analyzed using Ge as internal

Table 1
Experimental conditions used for the synthesis of $\text{Co}_x\text{Fe}_{3-x}\text{O}_4$ samples.

Sample	x nominal ^a	x effective ^b	Surfactant	Solvent
Fe	0	0	AO, OAM	Bn_2O
CoFe02	0.3	0.2	AO, OAM, HDD	Ph_2O
CoFe04	0.5	0.4	AO, OAM, HDD	Ph_2O
CoFe06	0.9	0.6	AO, OAM	Bn_2O
CoFe09	1	0.9	LA	Bn_2O
CoFe10	1	1	OAM	Bn_2O

^a x calculated from the Fe and Co precursors ratio.

^b x calculated from the Co:Fe ratio obtained from elemental analysis (ICP-AES).

standard. Calibration standards were prepared by gravimetric serial dilution from monostandards at 1000 mg L. The wavelengths used for Co, Fe, and Ge were 238.204, 238.892, and 209.426 nm, respectively.

2.3. Magnetic characterization

Magnetic measurements were performed using two SQUID magnetometers (Cryogenic Ltd. S600 and Quantum Design MPMS). Zero Field Cooled (ZFC) and Field Cooled (FC) magnetization measurements were performed as a function of the temperature applying a weak magnetic field ($H_{\text{probe}}=5$ mT) after cooling the sample in the absence (ZFC) and in the presence (FC) of H_{probe} . Powder samples were hosted in a Teflon sample holder and then pressed in a pellet in order to prevent preferential orientation of the nano-crystallites under the magnetic field. The diamagnetic contribution of the sample holder, which was separately measured in the same temperature and field ranges, was found negligible for all the samples.

Calorimetric measurements of Specific Absorption Rate (SAR) were performed using an experimental set-up made at the laboratory, composed by a power supply CELES[®] MP6/400 (FIVES CELES), a water-cooled heating station connected to the power supply and an induction coil. Measurements were carried out by applying for 300 s a magnetic field of 12 kA/m amplitude and 183 KHz frequency on a toluene suspension of magnetic NPs in the presence of 7.5 mM of OA and 7.5 mM of OAM. The concentrations of the suspension were 1.6% w/w for Fe and CoFeO₂; 1.8% w/w for CoFeO₄; 1.7% w/w for CoFeO₆; 1.1% w/w CoFeO₉ and 1.5% w/w for CoFeO₁₀. The field amplitude and the frequency were measured using a specific probe for high frequency magnetic field (AMF Life Systems[®]). The temperature of the sample was recorded by a temperature optical fiber probe (OPTOCON-FOTEMP) dipped into the solution. Samples were surrounded by polystyrene and hosted in a glass Dewar to ensure the proper thermal isolation.

3. Results and discussion

3.1. Synthesis and structural characterization.

A set of 8 nm non-stoichiometric cobalt ferrite, $\text{Co}_x\text{Fe}_{3-x}\text{O}_4$, with different Co content ($0 \leq x \leq 1.0$) was successfully synthesized by thermal decomposition of metal acetylacetonates in high-boiling solvents with a synthetic strategy modified from that used by Sun et al. [25]. The size was chosen close to the lowest limit of the range corresponding to the theoretical maximum of SAR expected for stoichiometric cobalt ferrite [7]. However, using OA, OAM and HDD as surfactants, we found that the Co:Fe ratio, determined by ICP-AES, was always lower than the nominal value, and, even by adding an excess of $\text{Co}(\text{acac})_2$ while keeping the total moles of metal (Fe+Co) unchanged, samples with $x > 0.6$ could not be obtained. A systematic Co depletion in $\text{Co}_x\text{Fe}_{3-x}\text{O}_4$ NPs synthesized by thermal decomposition of metal acetylacetonate precursors was already reported in the literature [26–28]. For instance, Barron et al. [26] performed a systematic investigation of the parameters involved in this synthesis and reported a constant Co reduction throughout the whole investigated composition range ($0.15 \leq x \leq 1.0$). Shemer et al. [27] attributed the Co depletion to the presence of the long chain diol, HDD, although we did not observe any difference when the reaction was repeated without this surfactant (Table 1). In addition, a statistical study on the synthesis of cobalt ferrite by thermal decomposition reaction identified the decrease of the reflux temperature as responsible for the reduction of the Co:Fe ratio, suggesting that the decomposition of the Co-precursor occurs at higher temperature than the Fe precursor [28].

In the present case, we found the surfactant plays a fundamental role in determining the final composition. Indeed, when the NPs were synthesized using LA alone or OAM alone, $\text{Co}_x\text{Fe}_{3-x}\text{O}_4$ with $x=0.9$ and $x=1.0$, respectively, were obtained. This result can be explained considering that a modification of the surfactant nature corresponds to a change in the decomposition temperature of the metal precursors.

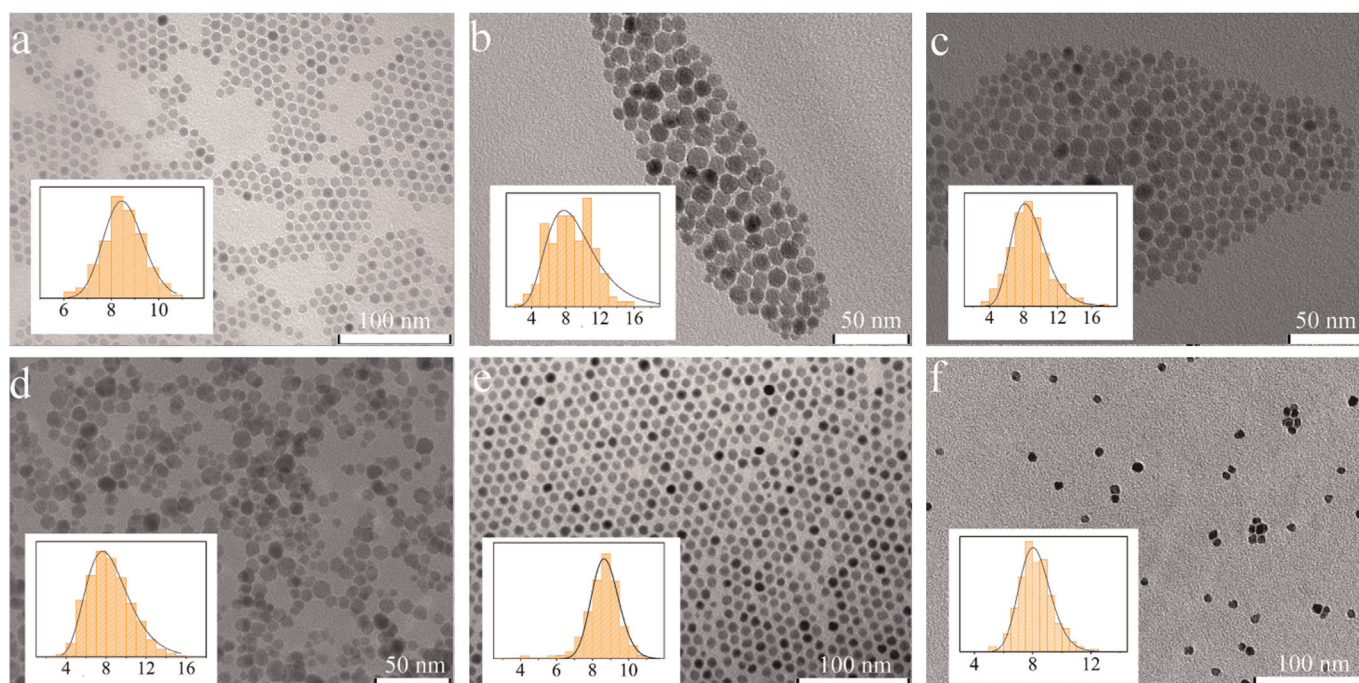


Fig. 1. TEM images of $\text{Co}_x\text{Fe}_{3-x}\text{O}_4$ NPs. (a) Fe ($d=8.3 \pm 0.9$ nm), (b) CoFeO₂ ($d=8.6 \pm 2.5$ nm), (c) CoFeO₄ ($d=8.6 \pm 2.2$ nm), (d) CoFeO₆ ($d=8.4 \pm 2.1$ nm), (e) CoFeO₉ ($d=8.6 \pm 0.6$ nm) and (f) CoFeO₁₀ ($d=8.2 \pm 1.1$ nm). Average size and standard deviation evaluated from the diameter histogram, shown in the inset, are reported in brackets. The best fit curve to a log-normal distribution is also reported as a continuous line.

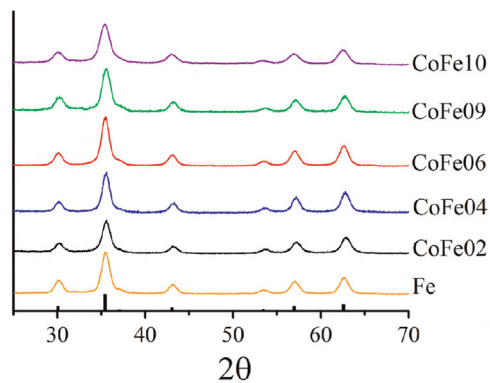


Fig. 2. XRD patterns of $\text{Co}_x\text{Fe}_{3-x}\text{O}_4$ NPs compared to the reference pattern of cobalt ferrite (black bars; PDF22-1086).

In Fig. 1 representative TEM images are reported together with the particle size distribution obtained from a statistical analysis over ca. 500–900 NPs. All samples are composed by uniform, spherical shaped NPs of diameter $d=8\text{--}8.5$ nm (Table 1). The size distribution can be nicely fitted to a log-normal function, as commonly observed for NPs prepared with wet-chemical techniques. The XRD diffraction patterns, reported in Fig. 2, well match in intensity and peak position those of cubic spinel oxides. In fact, the lattice parameters a , reported in Table 1, are close to the ones expected for magnetite (8.3963 Å) and cobalt ferrite (8.3919 Å). The crystallite diameters, d_{XRD} , obtained with the Scherrer analysis (Table 1), are comparable to those obtained by TEM measurements, suggesting that the particles can be considered as single crystals of high quality.

3.2. Hyperthermic and magnetic characterization.

The investigation of the hyperthermic efficiency of the $\text{Co}_x\text{Fe}_{3-x}\text{O}_4$ NPs was performed by evaluating the Specific Absorption Rate (SAR), i.e. the absorbed power per mass unit of the toluene suspension (1.1–1.8% w/w). The SAR values were estimated from the initial slope of the kinetic curves, $dT/dt(0)$, using the equation

$$\text{SAR} = \frac{1}{m_{\text{metal}}} \left(\sum_i c_i m_i \right) \frac{dT}{dt(0)} \quad (1)$$

where i denotes each species (solvent, surfactants and NPs), c_i the specific heat, m_i the mass and m_{metal} the total mass of metal. The field amplitude, $H_0=12$ kA/m, and frequency, $f=183$ kHz, were chosen such as their product undergoes the tolerance limit ($H_0 \cdot f=5 \times 10^9 \text{ A m}^{-1} \text{ s}^{-1}$) currently accepted in order to avoid any undesired side effects on human beings for small region exposure [29]. Larger amplitudes or frequencies can produce uncontrolled

Table 2
Chemical, structural and hyperthermic properties of $\text{Co}_x\text{Fe}_{3-x}\text{O}_4$.

Sample	x^a	d (nm) ^b	a (Å) ^c	d_{XRD} (nm) ^d	SAR (W/g metal) ^e
Fe	0	8.3 ± 0.9	8.3997 (9)	8.0 (0.1)	6.5 ± 0.5
CoFe02	0.2	8.6 ± 2.5	8.372 (3)	7.7 (0.2)	11.2 ± 1.0
CoFe04	0.4	8.6 ± 2.2	8.387 (5)	8.6 (0.2)	27.7 ± 2.1
CoFe06	0.6	8.4 ± 2.1	8.390 (1)	8.1 (0.1)	40.4 ± 3.5
CoFe09	0.9	8.6 ± 0.6	8.388 (1)	7.7 (0.2)	19.0 ± 0.9
CoFe10	1.0	8.2 ± 1.1	8.406 (1)	6.4 (0.1)	10.8 ± 1.9

^a Cobalt content obtained from ICP analysis.

^b NP average diameter and standard deviation obtained from TEM data.

^c Lattice parameter.

^d Crystallite average size obtained from XRD data analysis (accuracy is given in brackets).

^e SAR values obtained under an alternating magnetic field of 12 kA/m and 183 kHz; the data (mean \pm std) were obtained averaging over 3 measurements.

tissue overheating due to induced eddy currents and peripheral muscles stimulation.

In Fig. 3a, the experimental kinetic curves are shown, while the SAR values are reported in Table 2. Pure magnetite NPs of 8 nm provide poor heating effect, while a sizeable value is measured once NPs are doped even with a small amount of Co ions ($x=0.2$). Interestingly, the heating efficiency further increases with the amount of doping, reaches a maximum for $x=0.6$, but it drops down for larger x (Fig. 3b). The interpretation of this result requires the analysis of the magnetic properties of the samples as the heating power depends not only on the parameters of the external applied field, H_0 and f , but also on the magnetization of the material, M_s , and on the characteristic time of the magnetization reversal, τ :

$$\text{SAR} \propto f H_0 M_s^2 V \left[\frac{2\pi f \tau}{1 + (2\pi f \tau)^2} \right] \quad (2)$$

and

$$\tau = \tau_0 \exp \left(\frac{KV}{k_B T} \right) \quad (3)$$

V and K , being the NP average volume and the magnetic anisotropy constant, respectively. In (3) we have not considered the Brownian contribution since magnetic data indicates that it is negligible (see below).

In Fig. 4, the temperature dependence of the ZFC and FC magnetizations of the whole series are shown, while the blocking temperature, T_B , identified by the ZFC maximum, are reported in Table 3. The trend of T_B as a function of the Co content qualitatively reflects what observed for the SAR, even though the presence of a maximum cannot be revealed as the T_B for two samples (CoFe04 and CoFe06) are larger than the highest investigated temperature (310 K).

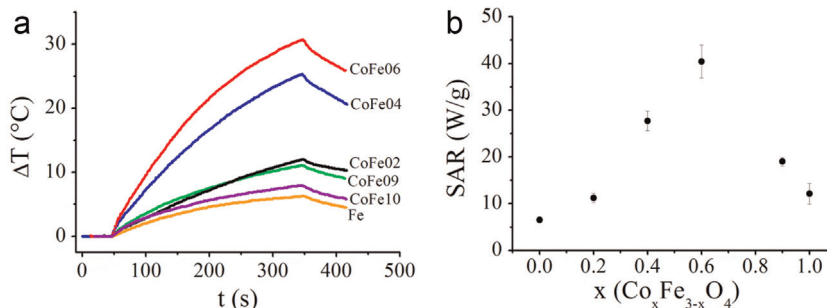


Fig. 3. (a) Kinetic curves and (b) corresponding SAR values of $\text{Co}_x\text{Fe}_{3-x}\text{O}_4$ NPs as a function of the cobalt content.

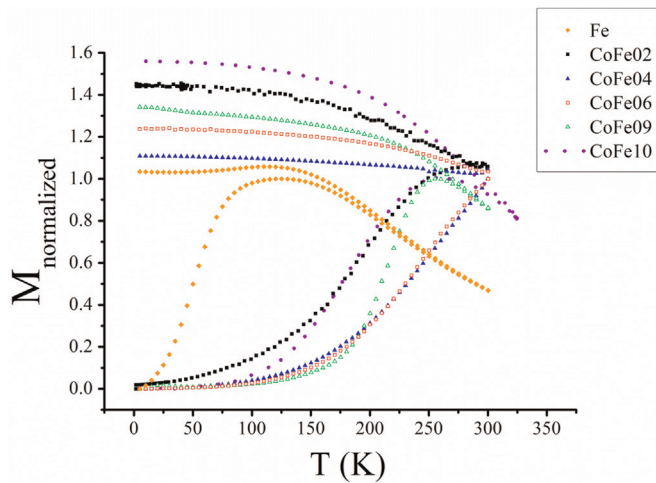


Fig. 4. Temperature dependence of the ZFC/FC magnetizations. Each curve is normalized to the corresponding ZFC maximum.

Table 3

Main magnetic parameters of the $\text{Co}_x\text{Fe}_{3-x}\text{O}_4$ samples.

Sample	T_B^a (K)	$\mu_0 H_C^b$ (T)	M_S^c 2.5 K (Am^2/kg)	M_{5T}/M_S^d 2.5 K (Am^2/kg)	M_R^e	M_S^f 300 K (Am^2/kg)	M_{5T}/M_S^g 300 K (Am^2/kg)
Fe	125	0.039	82	0.98	0.44	72	0.97
CoFe02	285	1.41	93	0.95	0.75	79	0.96
CoFe04	> 300	1.42	98	0.95	0.82	81	0.99
CoFe06	> 300	1.55	98	0.98	0.81	88	0.97
CoFe09	258	1.50	90	0.93	0.74	73	0.92
CoFe10	263	1.36	87	0.92	0.67	79	0.89

^a Blocking temperature.

^b Coercive field at 2.5 K.

^c Low temperature saturation magnetization estimated by fitting the high field data to the law $M = M_S + a/H + b/H^2$.

^d Low temperature magnetization at 5 T normalized to the saturation value.

^e Reduced remanent magnetization ($M_0 T/M_S T$).

^f Room temperature saturation magnetization.

^g Room temperature magnetization at 5 T normalized to the saturation value.

The field dependence of the magnetization was investigated both at low (2.5 K) and at room (300 K) temperature. All the samples do not display significant remanence nor coercivity at 300 K, while they show an hysteretic behavior at low temperature (Fig. 5a). At both temperatures the saturation is almost completely reached at the highest applied fields ($M_{5T}/M_S > 0.9$) and the magnetization of saturation is close to the bulk value, confirming the high crystallinity of the samples. It is generally found, indeed, that M_S decreases with reducing the material size because of the

formation of a spin-disordered layer at the NP surface, which, as it has been recently demonstrated [30], can be strongly influenced by the capping moieties that can partially restore the bulk environment. The reduced crystallite size of CoFe10, as evidenced by XRD data, and the different kind of capping ligand used for the preparation of CoFe09 can thus induce a decrease of the M_S which cannot be directly related to their Co content. In the final discussion, we will take into account that the M_S trend, again similar to the SAR one, may be partially ascribed to these accidental factors.

The coercive field at low temperature, H_C , presents a sharp increase once a small amount of Co is added, but no such significant variations are observed among the Co-doped samples, where again a trend similar to that of SAR can be observed. While large values of H_C generally denote highly anisotropic systems, the reduced remanence, $M_R = M_0 T/M_S T$, is correlated to the nature of the anisotropy symmetry, as $M_R = 0.5$ and $M_R = 0.83$ are foreseen for uniaxial and cubic anisotropy, respectively. For spinel ferrites, these two components are associated to the surface (uniaxial) and magneto-crystalline (cubic) terms of the total magnetic anisotropy [31]. In the present case, M_R exhibits a trend similar to the one observed for SAR, H_C and T_B (Table 3) suggesting that the cubic magneto-crystalline component is dominant for intermediate compositions.

The magnetic anisotropy constant, K , can be estimated from the low temperature coercive field H_C (Table 3) as, for an ensemble of randomly oriented NPs at a finite temperature T , $H_C = 0.96 \frac{K}{M_S} \left[1 - \left(\frac{T}{T_B} \right)^{0.77} \right]$. In our case, since the temperature-dependent term is negligible for all samples (T_B is always much larger than $T = 2.5$ K), the anisotropy constant can be simply estimated by $K = H_C M_S / 0.96$, where M_S is the value at 2.5 K. The obtained K values are always higher than the ones of the corresponding bulk materials [32], consistently with the presence of a surface anisotropy contribution which becomes relevant when the material is reduced to the nanoscale. For instance, for the extremes of the series Fe and CoFe10 K is $1.5 \times 10^4 \text{ J/m}^3$ and $5.7 \times 10^5 \text{ J/m}^3$, respectively, comparing to bulk magnetite ($1.3 \times 10^4 \text{ J/m}^3$) and cobalt ferrite ($2 \times 10^5 \text{ J/m}^3$) [33]. As expected from the H_C and M_S results, the so obtained K values (Fig. 5b) show that the maximum of the magnetic anisotropy is reached at $x = 0.6$. This result nicely confirms the one we previously observed on investigating the magnetic properties of a family of 5 nm maghemite NPs doped with different amount of Co [22]. Moreover, since the trend of K matches that of the remanence, it can be argued that K is mainly driven by the magneto-crystalline contribution, supporting the idea that such behavior is an intrinsic property of the doped nanomaterial.

The analysis of the magnetic properties has clearly shown how the SAR is related both to the magnetic moment and anisotropy, as they all exhibit the same trend with increasing Co content. However, it can be instructive to evaluate the relative weight of M_S and

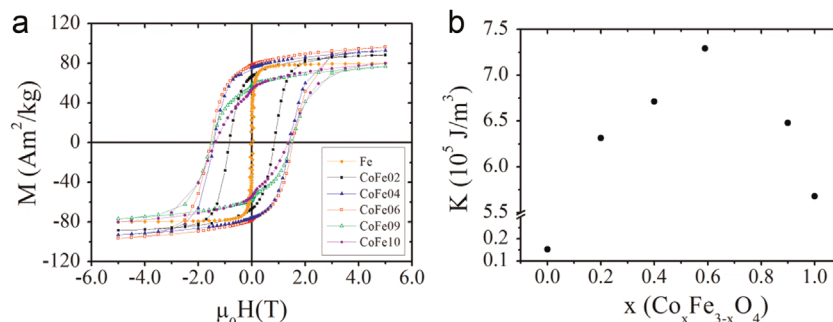


Fig. 5. (a) Low temperature field dependence of the magnetization, M , and (b) anisotropy constant, K , as a function of cobalt content.

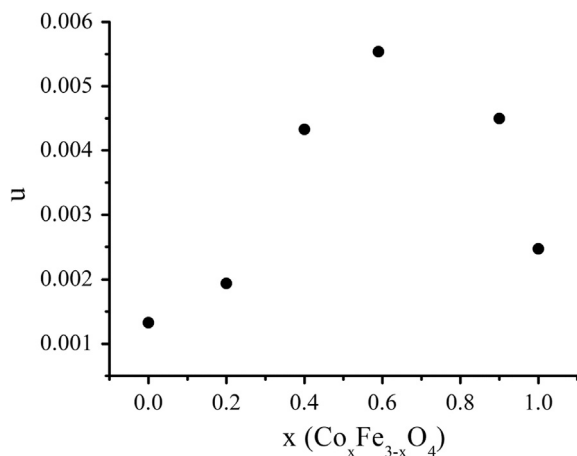


Fig. 6. Dependence of $u = SAR/M_s^2$ as a function of cobalt content.

K in the determination of the final hyperthermic efficiency. Unfortunately, this is not an easy task, since, while M_S can be directly obtained from the M vs. H curves at 300 K, the determination of the magnetic anisotropy at room temperature is more complex. Its value is indeed not accessible as neither hysteresis loops nor AC susceptibility measurements can be used, since part of the samples are blocked and part are unblocked at 300 K. Moreover, the large temperature dependence of K and the different variation expected for the various contributions to it prevent the use of the low temperature data shown in Fig. 5b [34]. However, the weight of K to the SAR can be tentatively estimated indirectly by removing the contribution of the saturation magnetization. In Fig. 6 the parameter $u = SAR/M_s^2$ is reported as a function of x : the obtained data maintain a similar percentage variation ($1 - u_{min}/u_{max}$) of SAR (ca. 80%), suggesting that the main contribution to the hyperthermic behavior arises from the magnetic anisotropy. This result underlines how for non-stoichiometric cobalt ferrite the heating power is fully determined by the magnetic features of the material intrinsically dependent on its Co-content. This further implies that in our samples the Brownian relaxation does not contribute to the heat dissipation mechanism, therefore allowing the control of the hyperthermic effect independently of any external parameter which, in the case of clinical application, are often unknown.

4. Conclusions

We reported the investigation of the structural, magnetic and hyperthermic properties of a series of 8 nm Co-doped magnetite NPs whose Co:Fe molar ratio has been varied systematically from 0 to 0.5 while keeping unchanged the mean diameter and the spherical morphology. The structural characterization displays that all the samples are composed of monodisperse and highly crystalline NPs. The SAR, evaluated on toluene dispersions of the NPs, increases with cobalt content up to $x=0.6$, and then decreases for larger x values. The magnetic measurements enlighten that this peculiar behavior can be ascribed to the magnetic anisotropy, quantified by the effective anisotropy constant, K . The whole magnetic data confirm what observed in our previous work on 5 nm Co_xFe_(8/3-2x/3)O₄ NPs: the highest cubic contribution to magnetic anisotropy and the maximum value of K are reached for intermediate composition. Thus, the best hyperthermic efficiency will be obtained for a partial substitution of Fe²⁺ ions with Co²⁺ in the spinel lattice of magnetite. Moreover, it is important to underline that, for Co_xFe_{3-x}O₄, a mean diameter of 8–8.5 nm is large enough for obtaining a significant heating applying field

amplitude and frequency compatible with clinical requirements, while magnetite of same size shows only poor hyperthermic efficiency. This result has a great interest for MFH application, since it allows for the reduction of the NP size guaranteeing the hyperthermic efficacy independently of environmental parameters, meanwhile increasing stability and circulation time in the body fluids, and thus the targeting capability.

Notes

The authors declare no competing financial interest.

Acknowledgments

The authors thank Dr. Samuele Ciattini and Dr. Francesca Loglio for their support in XRD measurements and Dr. Francesco Rugi and Prof. R. Udusti for ICP-AES measurements. Maurizio Passaponti is gratefully acknowledged for the realization of glassware equipment for hyperthermia instrumentation. The financial support of Italian MIUR through Project FIRB Riname RBAP114AMK, Fondazione Cariplo through Project no. 2013-0752 “Batman”, and INSTM-Regione Lombardia through Project MAG-NANO, is gratefully acknowledged.

References

- [1] Q.A. Pankhurst, J. Connolly, S.K. Jones, J. Dobson, Applications of magnetic nanoparticles in biomedicine, *J. Phys. D: Appl. Phys.* 36 (2003) R167–R181. <http://dx.doi.org/10.1088/0022-3727/36/13/201>.
- [2] Q.A. Pankhurst, N.T.K. Thanh, S.K. Jones, J. Dobson, Progress in applications of magnetic nanoparticles in biomedicine, *J. Phys. D: Appl. Phys.* 42 (2009) 224001. <http://dx.doi.org/10.1088/0022-3727/42/22/224001>.
- [3] M. Colombo, S. Carregal-Romero, M.F. Casula, L. Gutiérrez, M.P. Morales, I. B. Böhm, et al., Biological applications of magnetic nanoparticles, *Chem. Soc. Rev.* 41 (2012) 4306–4334. <http://dx.doi.org/10.1039/c2cs15337h>.
- [4] K. Maier-Hauff, F. Ulrich, D. Nestler, H. Niehoff, P. Wust, B. Thiesen, et al., Efficacy and safety of intratumoral thermotherapy using magnetic iron-oxide nanoparticles combined with external beam radiotherapy on patients with recurrent glioblastoma multiforme, *J. Neurooncol.* 103 (2011) 317–324. <http://dx.doi.org/10.1007/s11060-010-0389-0>.
- [5] M. Johannsen, B. Thiesen, P. Wust, A. Jordan, Magnetic nanoparticle hyperthermia for prostate cancer, *Int. J. Hyperth.* 26 (2010) 790–795. <http://dx.doi.org/10.3109/02656731003745740>.
- [6] C.C. Berry, Progress in functionalization of magnetic nanoparticles for applications in biomedicine, *J. Phys. D: Appl. Phys.* 42 (2009) 224003. <http://dx.doi.org/10.1088/0022-3727/42/22/224003>.
- [7] J.-P. Fortin, C. Wilhelm, J. Servais, C. Ménager, J.-C. Bacri, F. Gazeau, Size-sorted anionic iron oxide nanomagnets as colloidal mediators for magnetic hyperthermia, *J. Am. Chem. Soc.* 129 (2007) 2628–2635. <http://dx.doi.org/10.1021/ja067457e>.
- [8] L. Lartigue, C. Innocenti, T. Kalaivani, A. Awwad, M.D.M. Sanchez Duque, Y. Guari, et al., Water-dispersible sugar-coated iron oxide nanoparticles. An evaluation of their relaxometric and magnetic hyperthermia properties, *J. Am. Chem. Soc.* 133 (2011) 10459–10472. <http://dx.doi.org/10.1021/ja11448t>.
- [9] M. Gonzales-Weimuller, M. Zeisberger, K.M. Krishnan, Size-dependant heating rates of iron oxide nanoparticles for magnetic fluid hyperthermia, *J. Magn. Mater.* 321 (2009) 1947–1950. <http://dx.doi.org/10.1016/j.jmmm.2008.12.017>.
- [10] S. Purushotham, R.V. Ramanujan, Modeling the performance of magnetic nanoparticles in multimodal cancer therapy, *J. Appl. Phys.* 107 (2010) 114701. <http://dx.doi.org/10.1063/1.3432757>.
- [11] B. Mehdaoui, A. Meffre, J. Carrey, S. Lachaize, L.-M. Lacroix, M. Gougeon, et al., Optimal size of nanoparticles for magnetic hyperthermia: a combined theoretical and experimental study, *Adv. Funct. Mater.* 21 (2011) 4573–4581. <http://dx.doi.org/10.1002/adfm.201101243>.
- [12] M. Comes Franchini, G. Baldi, D. Bonacchi, D. Gentili, G. Giudetti, A. Lascialfari, et al., Bovine serum albumin-based magnetic nanocarrier for MRI diagnosis and hyperthermic therapy: a potential theranostic approach against cancer, *Small* 6 (2010) 366–370. <http://dx.doi.org/10.1002/sml.200901689>.
- [13] D.W. Hwang, D.S. Lee, S. Kim, Gene expression profiles for genotoxic effects of silica-free and silica-coated cobalt ferrite nanoparticles, *J. Nucl. Med.* 53 (2012) 106–112. <http://dx.doi.org/10.2967/jnumed.111.088443>.

- [14] N. Sanpo, J. Tharajak, Y. Li, C.C. Berndt, C. Wen, J. Wang, Biocompatibility of transition metal-substituted cobalt ferrite nanoparticles, *J. Nanopart. Res.* 16 (2014) 2510. <http://dx.doi.org/10.1007/s11051-014-2510-3>.
- [15] B. Peeples, V. Goonavar, C. Peeples, D. Spence, V. Parker, C. Bell, et al., Structural, stability, magnetic, and toxicity studies of nanocrystalline iron oxide and cobalt ferrites for biomedical applications, *J. Nanopart. Res.* 16 (2014) 2290. <http://dx.doi.org/10.1007/s11051-014-2290-9>.
- [16] A.B. Salunkhe, V.M. Khot, N.D. Thorat, M.R. Phadatare, C.I. Sathish, D. S. Dhawale, et al., Polyvinyl alcohol functionalized cobalt ferrite nanoparticles for biomedical applications, *Appl. Surf. Sci.* 264 (2013) 598–604. <http://dx.doi.org/10.1016/j.apsusc.2012.10.073>.
- [17] L. Horev-Azaria, G. Baldi, D. Beno, D. Bonacchi, U. Golla-Schindler, J. C. Kirkpatrick, et al., Predictive toxicology of cobalt ferrite nanoparticles: comparative in-vitro study of different cellular models using methods of knowledge discovery from data, *Part. Fibre Toxicol.* 10 (2013) 32. <http://dx.doi.org/10.1186/1743-8977-10-32>.
- [18] V. Georgiadou, C. Kokotidou, B. Le Droumaguet, B. Carbonnier, T. Choli-Papadopoulou, C. Dendrinou-Samara, Oleylamine as a beneficial agent for the synthesis of CoFe₂O₄ nanoparticles with potential biomedical uses, *Dalton Trans.* 43 (2014) 6377–6388. <http://dx.doi.org/10.1039/c3dt53179a>.
- [19] E.A. Schultz-Sikma, H.M. Joshi, Q. Ma, K.W. Macrenaris, A.L. Eckermann, V. P. Dravid, et al., Probing the chemical stability of mixed ferrites: implications for MR contrast agent design, *Chem. Mater.* 23 (2011) 2657–2664. <http://dx.doi.org/10.1021/cm200509g>.
- [20] G. Baldi, D. Bonacchi, M.C. Franchini, D. Gentili, G. Lorenzi, A. Ricci, et al., Synthesis and coating of cobalt ferrite nanoparticles: a first step toward the obtainment of new magnetic nanocarriers, *Langmuir* 23 (2007) 4026–4028. <http://dx.doi.org/10.1021/la063255k>.
- [21] E. Fantechi, C. Innocenti, M. Zanardelli, M. Fittipaldi, E. Falvo, M. Carbo, et al., A smart platform for hyperthermia application in cancer treatment: cobalt-doped ferrite nanoparticles mineralized in human ferritin cages, *ACS Nano* 8 (2014) 4705–4719. <http://dx.doi.org/10.1021/nn500454n>.
- [22] E. Fantechi, G. Campo, D. Carta, A. Corrias, C. de Julián Fernández, D. Gatteschi, et al., Exploring the effect of Co doping in fine maghemite nanoparticles, *J. Phys. Chem. C* 116 (2012) 8261–8270. <http://dx.doi.org/10.1021/jp300806j>.
- [23] M. Veverka, P. Veverka, O. Kaman, A. Lančok, K. Závěta, E. Pollert, et al., Magnetic heating by cobalt ferrite nanoparticles, *Nanotechnology* 18 (2007) 345704. <http://dx.doi.org/10.1088/0957-4484/18/34/345704>.
- [24] H.M. Joshi, Y.P. Lin, M. Aslam, P.V. Prasad, E.A. Schultz-Sikma, R. Edelman, et al., Effects of shape and size of cobalt ferrite nanostructures on their MRI contrast and thermal activation, *J. Phys. Chem. C: Nanomater. Interfaces* 113 (2009) 17761–17767. <http://dx.doi.org/10.1021/jp905776g>.
- [25] S. Sun, H. Zeng, D.B. Robinson, S. Raoux, P.M. Rice, S.X. Wang, et al., Mono-disperse MFe₂O₄ (M=Fe, Co, Mn) nanoparticles, *J. Am. Chem. Soc.* 126 (2004) 273–279. <http://dx.doi.org/10.1021/ja0380852>.
- [26] C.A. Crouse, A.R. Barron, Reagent control over the size, uniformity, and composition of Co–Fe–O nanoparticles, *J. Mater. Chem.* 18 (2008) 4146–4153. <http://dx.doi.org/10.1039/b806686h>.
- [27] G. Shemer, E. Tirosh, T. Livneh, G. Markovich, Tuning a colloidal synthesis to control Co²⁺ doping in ferrite nanocrystals, *J. Phys. Chem. C* 111 (2007) 14334–14338. <http://dx.doi.org/10.1021/jp0736793>.
- [28] V.L. Calero-DdelC, A.M. Gonzalez, C. Rinaldi, A statistical analysis to control the growth of cobalt ferrite nanoparticles synthesized by the thermodecomposition method, *J. Manuf. Sci. Eng.* 132 (2010) 030914. <http://dx.doi.org/10.1115/1.4001717>.
- [29] R. Hergt, S. Dutz, Magnetic particle hyperthermia—biophysical limitations of a visionary tumour therapy, *J. Magn. Magn. Mater.* 311 (2007) 187–192. <http://dx.doi.org/10.1016/j.jmmm.2006.10.1156>.
- [30] J. Salafranca, J. Gazquez, N. Pérez, A. Labarta, S.T. Pantelides, S.J. Pennycook, et al., Surfactant organic molecules restore magnetism in metal-oxide nanoparticle surfaces, *Nano Lett.* 12 (2012) 2499–2503. <http://dx.doi.org/10.1021/nl300665z>.
- [31] J.L. Dormann, D. Fiorani, E. Tronc, Magnetic relaxation in fine-particle systems, *XCVIII Adv. Chem. Phys.* XCVIII (1997) 283–494.
- [32] M. Tachiki, Origin of the magnetic anisotropy energy of cobalt ferrite, *Prog. Theor. Phys.* 23 (1960) 1055–1072.
- [33] E.P. Wohlfarth, *Ferromagnetic Materials: A Handbook on the Properties of Magnetically Ordered Substances.*, Elsevier, North-Holland, 1980.
- [34] C. de Julián Fernández, Influence of the temperature dependence of anisotropy on the magnetic behavior of nanoparticles, *Phys. Rev. B* 72 (2005) 054438. <http://dx.doi.org/10.1103/PhysRevB.72.054438>.